Rogue waves in coupled Hirota systems

Shihua Chen* and Lian-Yan Song
Department of Physics, Southeast University, Nanjing 211189, China
(Received 27 December 2012; published 20 March 2013)

Exact rogue wave solutions of the coupled Hirota equations are obtained by using a Darboux dressing transformation. An analysis of the spectral parameter condition shows that our coupled rogue waves, equal or unequal in background height, always exist no matter what parameters have been chosen for the starting plane waves. We demonstrate that, compared with the decoupled ones, the coupled rogue waves can appear in a rather striking way, i.e., one wave exhibits a centrally humped structure, while the other may feature one single hole in the center—a dark rogue wave structure. It is expected that these unusual rogue wave structures due to the two-wave coupling may help explain the extreme wave events in deep ocean or other nonlinear dispersive media.

DOI: 10.1103/PhysRevE.87.032910 PACS number(s): 05.45.Yv, 42.65.Tg, 47.20.Ky

I. INTRODUCTION

Freak or rogue waves, initially termed to describe extreme wave events that emerge in deep ocean [1,2], have recently attracted a significant surge of research activities on both experimental observations and theoretical predictions, in areas as diverse as hydrodynamics [3,4], capillary waves [5], optics [6–8], plasma physics [9], Bose-Einstein condensates [10], and even finance [11]. Fundamentally, aside from having a peak amplitude generally more than twice the significant wave height, rogue waves appear from nowhere and disappear without a trace [12]. Experiments show that the rogue waves appear to follow L-shaped statistics and can occur more frequently than they would according to ordinary Gaussian statistics [6,8]. Although uncertainty about their fundamental origins remains, there has been a consensus that rogue waves can be intimately related to some kind of breather solutions of the underlying evolution equations [3,4,13,14].

In the context of the $(1+1)$-dimensional nonlinear Schrödinger (NLS) equation, one family of breather-type solutions is the so-called Ma solitons [15], which breathe in the propagation dimension but are transversally localized. By contrast, there is another hierarchy of breather solutions, also known as Akhmediev breathers (ABs) [14,16,17], which instead breathe in the transverse dimension but are localized in the other dimension. Interestingly, by setting the breathing period of these two kinds of breathers to infinity, identical rational (or rogue wave) solutions that are localized in both dimensions can be obtained. The simplest rational solution is the Peregrine soliton, which was first found by Peregrine in 1983 as the limiting case of Ma solitons [18]. Experimental verification of this Peregrine soliton has been successfully carried out in a water wave tank [3] and in optical fibers [7], confirming that rogue waves occurring in reality can be described by such kinds of rational solutions.

Recently, rogue wave solutions in other more complex systems have been sought. Using the Darboux dressing technique [19,20] or Hirota bilinear method [21], researchers have reported exact rogue wave solutions in a variety of integrable equations such as the Hirota equation [22,23], the Sasa-Satsuma equation [24], and the Davey-Stewartson equation [25]. Also, rogue waves in coupled NLS equations (or the Manakov system) [26], coupled Gross-Pitaevskii equations [27], and coupled NLS Maxwell-Bloch equations [28] have been demonstrated. Additionally, although rogue waves have been studied mostly in conservative systems, there appears to be an increasing number of experimental and theoretical works [8,29,30] that place an emphasis on the role of active media and dissipative systems so as to excite instabilities for the formation of rogue waves [13,14,31].

In this work we deal with the rogue wave solutions of the coupled Hirota (CH) equations [32–34]. Compared with the simple Manakov system [26], the CH system involves high-order effects such as third-order dispersion (TOD), self-steepening, and delayed nonlinear response and thus can be thought of as a more accurate prototype of the wave evolution in the real world. As an example, the CH equations can model the interaction of two waves brought on by severe weather in deep ocean [2,22] and as well as describe the propagation of ultrashort optical pulses in a birefringent fiber or simultaneous propagation of two fields in a nonlinear channel [33,34]. Since early works dealt with only solitonlike solutions [32–34], we present here the lowest-order but most general rogue wave solutions using the Darboux dressing technique [19,20]. Furthermore, the spectral parameters responsible for such coupled rogue waves and the related wave characteristics will be thoroughly discussed.

For the present study we write the CH equations in dimensionless form [32–34]

$$iu_t + \tfrac{1}{2}u_{xx} + (|u|^2 + |v|^2)u + i\epsilon[u_{xxx} + (6|u|^2 + 3|v|^2)u_x + 3uv^*v_x] = 0, \quad (1)$$

$$iv_t + \tfrac{1}{2}v_{xx} + (|v|^2 + |u|^2)v + i\epsilon[v_{xxx} + (6|v|^2 + 3|u|^2)v_x + 3vu^*u_x] = 0, \quad (2)$$

where $u(t,x)$ and $v(t,x)$ are the complex envelopes of the two fields, t is the evolution variable, and x is a second independent variable. The subscripts stand for the partial derivatives and the real parameter ϵ scales the integrable perturbations of the coupled NLS equations [26]. The terms included in the square brackets explain effects such as TOD, self-steepening, and delayed nonlinear response. It should be pointed out that the meaning of the dependent variables $u(t,x)$ and $v(t,x)$ and

*cshua@seu.edu.cn

 ©2013 American Physical Society

of coordinates t and x depends on the particular applicative context. For example, in deep water, $u(t,x)$ and $v(t,x)$ are the complex amplitudes related to the surface elevation with t and x being the time and longitudinal coordinates, respectively [1–4], while in optical fibers $u(t,x)$ and $v(t,x)$ represent the interacting optical fields or the two components of the vector optical field, with t being the propagation distance and x the time scaling the pulse duration [35].

II. DARBOUX DRESSING TRANSFORMATION

We note that Eqs. (1) and (2) pass the Painlevé test for integrability [33,36,37] and thus can be cast into a 3×3 linear eigenvalue problem

$$\mathbf{R}_x = \mathbf{U}\mathbf{R}, \quad \mathbf{R}_t = \mathbf{V}\mathbf{R}, \tag{3}$$

where $\mathbf{R} = (r,s,w)^{\mathsf{T}}$ (T means a matrix transpose) and

$$\mathbf{U} = \lambda\mathbf{U}_0 + \mathbf{U}_1, \tag{4}$$

$$\mathbf{V} = \lambda^3\mathbf{V}_0 + \lambda^2\mathbf{V}_1 + \lambda\mathbf{V}_2 + \mathbf{V}_3, \tag{5}$$

with

$$\mathbf{U}_0 = \frac{1}{12\epsilon}\begin{pmatrix} -2i & 0 & 0 \\ 0 & i & 0 \\ 0 & 0 & i \end{pmatrix}, \quad \mathbf{U}_1 = \begin{pmatrix} 0 & -u & -v \\ u^* & 0 & 0 \\ v^* & 0 & 0 \end{pmatrix}, \tag{6}$$

$$\mathbf{U}_2 = \begin{pmatrix} -(|u|^2+|v|^2) & u_x & v_x \\ u_x^* & |u|^2 & vu^* \\ v_x^* & uv^* & |v|^2 \end{pmatrix}, \tag{7}$$

$$\mathbf{U}_3 = \begin{pmatrix} e_1+e_2 & e_3 & e_4 \\ -e_3^* & -e_1 & e_5 \\ -e_4^* & -e_5^* & -e_2 \end{pmatrix}, \tag{8}$$

$$\mathbf{V}_0 = \frac{1}{16\epsilon}\mathbf{U}_0, \quad \mathbf{V}_1 = \frac{1}{8\epsilon}\mathbf{U}_0 + \frac{1}{16\epsilon}\mathbf{U}_1, \tag{9}$$

$$\mathbf{V}_2 = \frac{1}{8\epsilon}\mathbf{U}_1 - \frac{i}{4}\mathbf{U}_2, \quad \mathbf{V}_3 = \epsilon\mathbf{U}_3 - \frac{i}{2}\mathbf{U}_2. \tag{10}$$

Here λ is the complex spectral parameter. The matrix elements in $\mathbf{U}_3$ are given by $e_1 = uu_x^* - u^*u_x$, $e_2 = vv_x^* - v^*v_x$, $e_3 = u_{xx} + 2u(|u|^2+|v|^2)$, $e_4 = v_{xx} + 2v(|u|^2+|v|^2)$, and $e_5 = u^*v_x - vu_x^*$. It is easy to prove that by virtue of the matrices (4) and (5), the CH equations (1) and (2) can be exactly reproduced from the compatibility condition $\mathbf{U}_t - \mathbf{V}_x + \mathbf{U}\mathbf{V} - \mathbf{V}\mathbf{U} = 0$.

The Darboux dressing process [19,20] can be simply formulated as follows. First, suppose u and v are a pair of known solutions of Eqs. (1) and (2); one can use them as initial potentials and find the eigenfunction $\mathbf{R}$ through the Lax pair (3). Then, in terms of $\mathbf{R}$ for a given spectral parameter, a dress operator $\mathbf{D}$ is properly constructed with which $\mathbf{R}$ can be dressed into $\mathbf{R}'$ (i.e., $\mathbf{R}' = \mathbf{D}\mathbf{R}$) and, moreover, $\mathbf{R}'$ satisfies the Lax pair (3) of the same form but with a new pair of potentials u' and v'. Finally, u' and v' are thought to be a new pair of solutions to Eqs. (1) and (2) if and only if

$$\mathbf{U}(u',v',\lambda) = \mathbf{D}[-\partial_x + \mathbf{U}(u,v,\lambda)]\mathbf{D}^{-1}, \tag{11}$$

$$\mathbf{V}(u',v',\lambda) = \mathbf{D}[-\partial_t + \mathbf{V}(u,v,\lambda)]\mathbf{D}^{-1}. \tag{12}$$

Note that here we use $\mathbf{M}(u',v',\lambda)$ ($\mathbf{M} = \mathbf{U},\mathbf{V}$) to represent a transformed matrix identical to $\mathbf{M}(u,v,\lambda)$ but only with $u \leftrightarrow u'$ and $v \leftrightarrow v'$ interchanged correspondingly.

As in Ref. [20], the Darboux dressing operator can be correctly defined with the form

$$\mathbf{D} = \mathbf{I} - \frac{\lambda_1 - \lambda_1^*}{\lambda - \lambda_1^*}\mathbf{X}, \tag{13}$$

$$\mathbf{D}^{-1} = \mathbf{I} + \frac{\lambda_1 - \lambda_1^*}{\lambda - \lambda_1}\mathbf{X}^\dagger, \tag{14}$$

where λ_1 is any given value of the spectral parameter λ, $\mathbf{I}$ is a 3×3 identity matrix, the dagger indicates the complex-conjugate transpose, and $\mathbf{X}$ is a 3×3 rank-deficient matrix given by

$$\mathbf{X} = \frac{1}{\Pi}\mathbf{R}(\lambda_1)\mathbf{R}(\lambda_1)^\dagger, \tag{15}$$

with $\Pi = \mathbf{R}(\lambda_1)^\dagger\mathbf{R}(\lambda_1) = |r(t,x,\lambda_1)|^2 + |s(t,x,\lambda_1)|^2 + |w(t,x,\lambda_1)|^2$. It follows easily from Eqs. (13)–(15) that $\mathbf{X} = \mathbf{X}^\dagger = \mathbf{X}^2$ and $\mathbf{D}\mathbf{D}^{-1} = \mathbf{I}$. With this in mind and recalling that $\mathbf{U}(\lambda_1)^\dagger = -\mathbf{U}(\lambda_1^*)$ and $\mathbf{V}(\lambda_1)^\dagger = -\mathbf{V}(\lambda_1^*)$, one can verify that Eqs. (11) and (12) are completely satisfied. In particular, Eq. (11) can be exactly reduced to

$$\mathbf{U}_1(u',v') = \mathbf{U}_1(u,v) - (\lambda_1 - \lambda_1^*)(\mathbf{X}\mathbf{U}_0 - \mathbf{U}_0\mathbf{X}), \tag{16}$$

which, according to Eq. (6), gives rise to the auto-Darboux transformation between the new and the seeding solutions:

$$u' = u + \frac{i(\lambda_1 - \lambda_1^*)}{4\epsilon\Pi}r(t,x,\lambda_1)s^*(t,x,\lambda_1), \tag{17}$$

$$v' = v + \frac{i(\lambda_1 - \lambda_1^*)}{4\epsilon\Pi}r(t,x,\lambda_1)w^*(t,x,\lambda_1). \tag{18}$$

In other words, by an appropriate choice of seeding solutions, Eqs. (17) and (18) can yield a hierarchy of soliton or breather-type solutions of the CH equations. Obviously, the larger the order of the solutions, the more complicated their forms are. In the following we are concerned only with the lowest-order (fundamental) rogue wave solutions.

III. EXACT COUPLED ROGUE WAVE SOLUTIONS

It is well known that rogue wave solutions correspond to the limiting case of either Ma solitons or ABs, which are homoclinically or heteroclinically related to the unstable plane waves [19,20,22,24]. Therefore, we start directly with a general pair of plane-wave solutions

$$u_0(t,x) = \frac{c_1}{2\epsilon}\exp\left[-\frac{i}{2\epsilon}\left(k_1x - \frac{\omega_1}{4\epsilon}t\right)\right], \tag{19}$$

$$v_0(t,x) = \frac{c_2}{2\epsilon}\exp\left[-\frac{i}{2\epsilon}\left(k_2x - \frac{\omega_2}{4\epsilon}t\right)\right], \tag{20}$$

where $c_n,k_n,\omega_n \in \mathbb{R}$ ($n = 1,2$) and the dispersion relations read

$$\omega_1 = 2\alpha - k_1^2 - k_1^3 + 6c_1^2k_1 + 3c_2^2\kappa, \tag{21}$$

$$\omega_2 = 2\alpha - k_2^2 - k_2^3 + 6c_2^2k_2 + 3c_1^2\kappa. \tag{22}$$

Here and for later use we define $\alpha = c_1^2 + c_2^2$, $\beta = c_1^2 - c_2^2$, $\kappa = k_1 + k_2$, and $\delta = k_1 - k_2$.

We are mainly interested in the coupled situation $\delta \neq 0$. If $\delta = 0$, Eqs. (1) and (2) will be decoupled into two single Hirota equations. We will discuss this simple decoupled case in Sec. V.

Now, substituting Eqs. (19) and (20) into Eq. (3), with some manipulations we obtain

$$r(t,x,\lambda) = e^{-i\theta_1} + \Gamma_1 e^{-i\theta_2} + \Gamma_2 e^{-i\theta_3}, \tag{23}$$

$$s(t,x,\lambda) = \frac{2\epsilon}{c_1} f_1 u_0^*(t,x) r(t,x,\lambda), \tag{24}$$

$$w(t,x,\lambda) = \frac{2\epsilon}{c_2} f_2 v_0^*(t,x) r(t,x,\lambda), \tag{25}$$

where Γ_1 and Γ_2 are arbitrary constants and

$$\theta_j = \frac{\mu_j}{12\epsilon} x + \frac{\nu_j}{288\epsilon^2} t, \tag{26}$$

$$\begin{aligned}\nu_j = {} & \left[\lambda^2 - (\kappa-2)\lambda - 12\alpha + \tfrac{3}{2}(\delta^2 - \kappa^2)\right]\mu_j \\ & + \left(\frac{\lambda}{2} + \kappa + 1\right)\mu_j^2 - \lambda^3 - 2(\kappa+1)\lambda^2 \\ & - 3(4\alpha + \delta^2 - \kappa^2)\lambda - 72\alpha(\kappa+1) - 36\delta\beta,\end{aligned} \tag{27}$$

$$f_1 = \frac{r_{11}e^{-i\theta_1} + \Gamma_1 r_{12} e^{-i\theta_2} + \Gamma_2 r_{13} e^{-i\theta_3}}{e^{-i\theta_1} + \Gamma_1 e^{-i\theta_2} + \Gamma_2 e^{-i\theta_3}}, \tag{28}$$

$$f_2 = \frac{r_{21}e^{-i\theta_1} + \Gamma_1 r_{22} e^{-i\theta_2} + \Gamma_2 r_{23} e^{-i\theta_3}}{e^{-i\theta_1} + \Gamma_1 e^{-i\theta_2} + \Gamma_2 e^{-i\theta_3}}, \tag{29}$$

with

$$r_{1j} = \frac{6ic_1}{\mu_j + \lambda - 6k_1}, \quad r_{2j} = \frac{6ic_2}{\mu_j + \lambda - 6k_2}. \tag{30}$$

The index j in Eqs. (26), (27), and (30) runs over 1, 2, and 3 and μ_j are three roots of the cubic equation

$$(\mu - 2\kappa)^3 - 3\sigma(\mu - 2\kappa) + 2\rho = 0, \tag{31}$$

where the coefficients σ and ρ are defined by

$$\sigma(\lambda) = (\kappa - \lambda)^2 + 3\delta^2 + 12\alpha, \tag{32}$$

$$\rho(\lambda) = (\kappa - \lambda)^3 + 9(\kappa - \lambda)(2\alpha - \delta^2) - 54\delta\beta. \tag{33}$$

In an orderly way, we can write the formulas of the three roots of Eq. (31) as

$$\mu_1(\lambda) = -\frac{1}{2}\left(\ell + \frac{\sigma}{\ell}\right) - i\frac{\sqrt{3}}{2}\left(\ell - \frac{\sigma}{\ell}\right) + 2\kappa, \tag{34}$$

$$\mu_2(\lambda) = -\frac{1}{2}\left(\ell + \frac{\sigma}{\ell}\right) + i\frac{\sqrt{3}}{2}\left(\ell - \frac{\sigma}{\ell}\right) + 2\kappa, \tag{35}$$

$$\mu_3(\lambda) = \ell + \frac{\sigma}{\ell} + 2\kappa, \tag{36}$$

where

$$\ell = (-\rho + \sqrt{\rho^2 - \sigma^3})^{1/3}.$$

It is clear that these three roots, along with σ and ρ, are functions of the spectral parameter λ. Obviously, if choosing a specific parameter $\lambda = \lambda'$ so that

$$\ell(\lambda') = \sqrt{\sigma(\lambda')} \tag{37}$$

or, more explicitly [via Eqs. (32) and (33)],

$$\rho(\lambda') + [\sqrt{\sigma(\lambda')}]^3 = 0, \tag{38}$$

we then get two equal roots

$$\mu_1(\lambda') = \mu_2(\lambda') = -\ell(\lambda') + 2\kappa \tag{39}$$

and the third root

$$\mu_3(\lambda') = 2\ell(\lambda') + 2\kappa. \tag{40}$$

It should be noted that as $\ell(\lambda') = -\sqrt{\sigma(\lambda')}$ or, equivalently, $\rho(\lambda') = [\sqrt{\sigma(\lambda')}]^3$, one can also get two equal roots given by Eq. (39). However, as one can verify, this condition can result in the same rogue wave solutions as derived from Eq. (37) or (38). For this reason, we consider only Eqs. (37) and (38) in our study.

It is now very straightforward to derive the rogue wave solutions. Specifically, in Eqs. (28) and (29), we set $\Gamma_1 = -1$ and $\Gamma_2 = 0$. Hence, in the limit of $\lambda = \lambda'$, f_1 and f_2 can take the forms

$$\lim_{\lambda=\lambda'} f_1 = r_{11}(\lambda') + \frac{16\epsilon^2[6k_2 + \lambda' - 2\mu_1(\lambda')]}{c_1\delta\chi} \equiv F, \tag{41}$$

$$\lim_{\lambda=\lambda'} f_2 = r_{21}(\lambda') - \frac{16\epsilon^2[6k_1 + \lambda' - 2\mu_1(\lambda')]}{c_2\delta\chi} \equiv G, \tag{42}$$

where χ is a linear function of t and x, given by

$$\begin{aligned}\chi = {} & [2(\lambda' + 2\kappa + 2)\mu_1(\lambda') + 2\lambda'(\lambda' - \kappa + 2) \\ & - 3(\kappa^2 - \delta^2 + 8\alpha)]t + 48\epsilon x.\end{aligned} \tag{43}$$

Here $\mu_1(\lambda')$ is given by Eq. (39) and thereby $r_{11}(\lambda')$ and $r_{21}(\lambda')$ are determined by Eq. (30) with $\lambda = \lambda'$ and $j = 1$. Under these circumstances, f_1 and f_2 become two rational functions rather than exponential or periodic ones. This implies that when inserting Eqs. (23)–(25) into Eqs. (17) and (18), the new pair of solutions u' and v' can be identified as genuine rogue waves.

Consequently, by noting that $\Pi = |r(t,x,\lambda')|^2(1 + |F|^2 + |G|^2)$, we write the rogue wave solutions as

$$u(t,x) = u_0(t,x)\left[1 + \frac{i(\lambda' - \lambda'^*)F^*}{2c_1(1 + |F|^2 + |G|^2)}\right], \tag{44}$$

$$v(t,x) = v_0(t,x)\left[1 + \frac{i(\lambda' - \lambda'^*)G^*}{2c_2(1 + |F|^2 + |G|^2)}\right], \tag{45}$$

which, as one can verify, exactly satisfy the CH equations (1) and (2). It is worth noting that if $u(t,x)$ and $v(t,x)$ are a pair of solutions of Eqs. (1) and (2), so are $u(t,x+\iota)\exp(im)$ and $v(t,x+\iota)\exp(in)$, where ι, m, and n are arbitrary real constants. As such, in order to be more compact, the solutions (44) and (45) are sometimes translated along the x axis, with their constant phases being discarded completely. It is also worth noting that the spectral parameter λ' should be complex with a nonvanishing imaginary part, otherwise Eqs. (44) and (45) are still a pair of trivial plane-wave solutions. Fortunately, by solving Eq. (38), the allowed spectral parameter λ' is always found to be complex with $\mathrm{Im}(\lambda') \neq 0$, independently of what parameters in Eqs. (19) and (20) have been exploited, as shown in the following section.

IV. SPECTRAL PARAMETERS FOR COUPLED ROGUE WAVES

The condition (38) allows two solutions of λ' that fulfill $\mu_1(\lambda') = \mu_2(\lambda')$. In fact, it is equivalent to a real coefficient

quartic equation specified by $\rho^2(\lambda') - \sigma^3(\lambda') = 0$, despite the latter having introduced two additional roots. We can write this quartic equation as

$$\xi^4 + p\xi^2 + q\xi + a = 0, \tag{46}$$

where $\xi = \lambda' - \kappa - \beta/\delta$ and p, q, and a are given by

$$p = \frac{2(2\alpha^2 - \delta^4 + 10\delta^2\alpha - 3\beta^2)}{\delta^2}, \tag{47}$$

$$q = \frac{8\beta[(\alpha - 2\delta^2)^2 - \beta^2]}{\delta^3}, \tag{48}$$

$$a = \frac{(4\alpha + \delta^2)^3}{\delta^2} + \frac{(4\alpha^2 - 52\delta^2\alpha - 74\delta^4)\beta^2 - 3\beta^4}{\delta^4}. \tag{49}$$

After relaxing the condition (38) to Eq. (46), one should keep in mind that only two of its four roots are significant. Below we solve for the roots that are responsible for the coupled rogue waves according to two categories: (i) equal background amplitude $\beta = 0$ and (ii) unequal background amplitude $\beta \neq 0$. The complex nature of the roots, with illustrative examples, is also shown.

A. Equal background amplitude $\beta = 0$

We first consider the case of $\beta = 0$, which means that the coupled rogue waves have the same background height. For this case, Eq. (46) gives two simple spectral parameters that can meet the condition (38). Specifically, as $\alpha < 2\delta^2$, these two spectral parameters λ' take the form

$$\lambda' = \kappa - \frac{1}{|\delta|}\sqrt{\delta^4 - 2\alpha^2 - 10\delta^2\alpha \pm 2i\sqrt{\alpha(2\delta^2 - \alpha)^3}}; \tag{50}$$

otherwise they are determined by

$$\lambda' = \kappa \pm \frac{i}{|\delta|}\sqrt{2\alpha^2 + 10\delta^2\alpha - \delta^4 \pm 2\sqrt{\alpha(\alpha - 2\delta^2)^3}}. \tag{51}$$

Another two unwanted roots of Eq. (46) have been abandoned. By inspecting the radical parts in Eqs. (50) and (51), one can conclude that both spectral parameters are always complex regardless of whether $\alpha < 2\delta^2$ or $\alpha \geqslant 2\delta^2$. Hence the coupled rogue waves, defined by the spectral parameters (50) or (51), exist for all equal background scenarios.

A special note of interest here is the situation $\alpha = 2\delta^2$, where, according to Eq. (51), the spectral parameters take the form

$$\lambda' = \kappa \pm i3\sqrt{3}\delta. \tag{52}$$

In this situation $\sigma(\lambda') = \rho(\lambda') = 0$ and thus, according to Eqs. (37)–(40), we now have three equal real roots

$$\mu_1(\lambda') = \mu_2(\lambda') = \mu_3(\lambda') = 2\kappa. \tag{53}$$

As a result, with some manipulations, the rogue wave solutions (44) and (45) can reduce to

$$u(t,x) = u_0(t,x)(i + 96\epsilon^2\phi_2), \tag{54}$$

$$v(t,x) = v_0(t,x)(i + 96\epsilon^2\phi_1), \tag{55}$$

where ϕ_j $(j = 1,2)$ are given by

$$\phi_j = \frac{6\delta^2(3\kappa + 2)t + (-1)^j\delta\eta - 32i\epsilon^2}{36\delta^4(3\kappa + 2)^2t^2 + 3\delta^2\eta^2 + 1024\epsilon^4}, \tag{56}$$

with $\eta = (3\kappa^2 + 4\kappa - 33\delta^2)t + 16\epsilon x$. Noting that in deriving Eqs. (54) and (55) we have discarded the constant phase and translated the solutions along the x axis to make their central maximums close to the origin. It is obvious that this pair of rational solutions is localized in both space and time and thus describes a unique wave event that appears from nowhere.

An inspection of the extremums of the rogue wave amplitude indicates that our rogue wave solutions (54) and (55) have two interesting features. First, both rogue waves have a peak amplitude just twice that of the background. Second, either of the coupled rogue waves has two characteristic holes where the wave amplitude can fall to zero in the hole center; specifically, the u wave amplitude goes to zero at the two points in the plane (t,x):

$$\left(\tau_0, -\frac{\sqrt{2}\epsilon(1 + \zeta_0)}{\delta}\right), \quad \left(-\tau_0, \frac{\sqrt{2}\epsilon(1 + \zeta_0)}{\delta}\right), \tag{57}$$

whereas the v wave vanishes completely at

$$\left(\tau_0, \frac{\sqrt{2}\epsilon(1 - \zeta_0)}{\delta}\right), \quad \left(-\tau_0, -\frac{\sqrt{2}\epsilon(1 - \zeta_0)}{\delta}\right). \tag{58}$$

Here the parameters τ_0 and ζ_0 are defined as

$$\tau_0 = \frac{8\sqrt{2}\epsilon^2}{3\delta^2(3\kappa + 2)}, \quad \zeta_0 = \frac{3\kappa^2 + 4\kappa - 33\delta^2}{6\delta(3\kappa + 2)}.$$

Note that if $\kappa = -2/3$, the zero-amplitude points (57) and (58) will be at infinity. In such a special case, one can show that Eqs. (54) and (55) are a pair of line rogue waves [25] or, more accurately, a pair of algebraic solitons on their respective backgrounds [38].

Figure 1 displays the coupled rogue waves (54) and (55) with the starting plane-wave parameters being chosen such that $\alpha = 2\delta^2$ and $\beta = 0$. It can be clearly seen that both rogue waves contain two zero-amplitude holes separated by one wall-like hump in the center and moreover the hump has a peak amplitude exactly twice that of the background [see

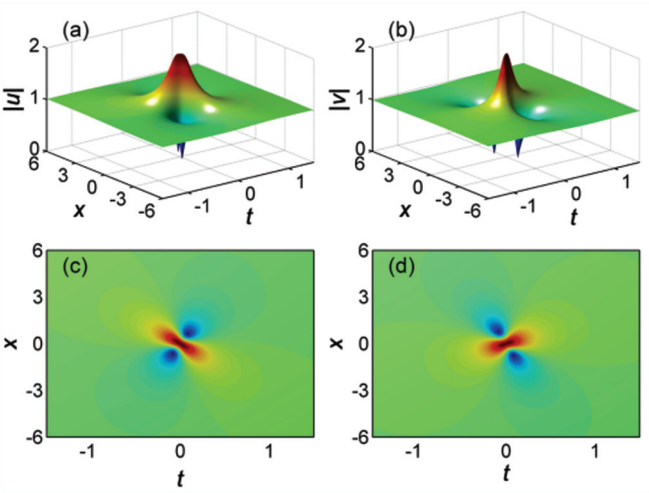

FIG. 1. (Color online) Coupled rogue waves (54) and (55) associated with $\lambda' = 3 \pm i3\sqrt{3}$ for the starting plane-wave parameters $\epsilon = 0.5$, $k_1 = 1$, $k_2 = 2$, $c_1 = 1$, and $c_2 = 1$. The values of ω_1 and ω_2 are given by Eqs. (21) and (22). (a) and (c) show the u wave and (b) and (d) show the v wave.

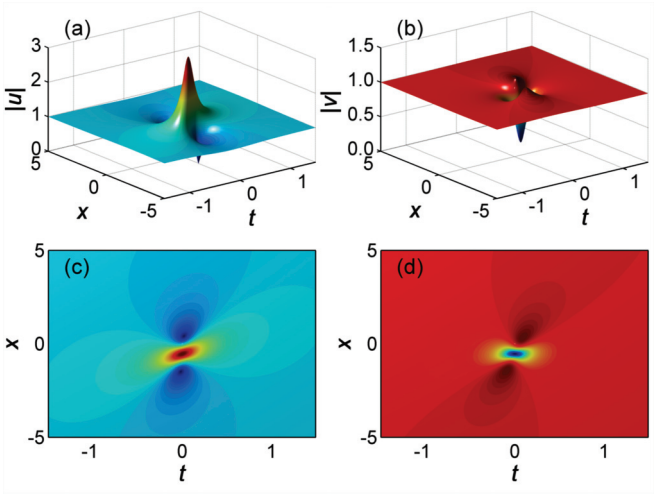

FIG. 2. (Color online) Pair of centrally humped and sunken rogue waves associated with $\lambda' = 4 - \sqrt{-18 + 6i\sqrt{3}}$ for the starting plane-wave parameters $\epsilon = 0.5$, $k_1 = 1$, $k_2 = 3$, $c_1 = 1$, and $c_2 = 1$. (a) and (c) show the u wave and (b) and (d) show the v wave.

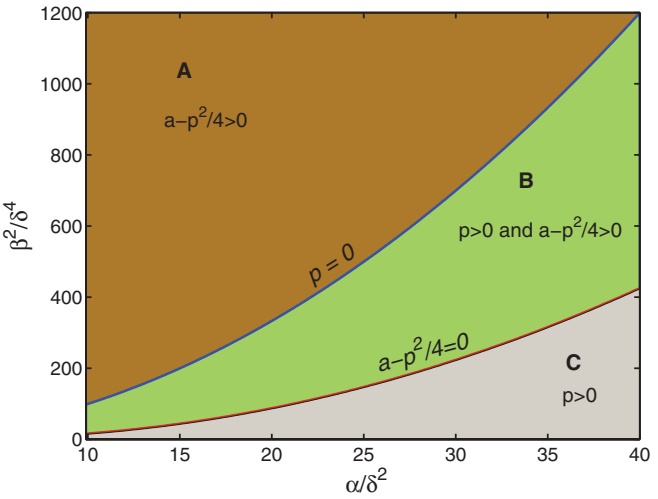

FIG. 3. (Color online) Allowed regimes of the condition $p > 0$ or $a - p^2/4 > 0$ in the plane $(\alpha/\delta^2, \beta^2/\delta^4)$ for $\alpha \geqslant (5 + 2\sqrt{6})\delta^2$ (only up to $40\delta^2$ is shown here). The blue and red lines, which represent $p = 0$ and $a - p^2/4 = 0$, respectively, separate the plane into three blocks A, B, and C with each identified by the corresponding condition inside.

Figs. 1(a) and 1(b)]. The hole centers of each rogue wave are exactly determined by Eq. (57) or (58) [see Figs. 1(c) and 1(d)]. Obviously, this pair of rogue waves, although somewhat alike in structure, distinguishes itself in zero-amplitude points and in a tilted angle.

More interestingly, an increase of the wave-number difference $|\delta|$ invalidating the relation $\alpha = 2\delta^2$ can lead to a new phenomenon: One rogue wave is amplified in peak amplitude while the other exhibits a deep submergence (dark rogue wave structure) in the center, as seen in Fig. 2. In this situation, one should use Eq. (50) or (51) to determine the spectral parameter λ' and correspondingly Eqs. (44) and (45) to describe the dynamics of the coupled rogue waves. We show that compared to those in Fig. 1, the u wave, which still contains two zero-amplitude holes, has been amplified in peak amplitude from 2 to 2.978 [see Figs. 2(a) and 2(c)], while the v wave features one hole in the center [see Figs. 2(b) and 2(d)]. If $\delta > 0$, the reverse applies, namely, the u wave is centrally sunken, but the v wave is humped there. Calculations show that such a dark rogue wave structure indeed results from the complete merger of two nearby holes as $|\delta|$ increases and, moreover, the larger the value of $|\delta|$, the shallower the depth of the central hole will become.

B. Unequal background amplitude $\beta \neq 0$

We now discuss the general case $\beta \neq 0$. It is noted that as $\beta^2 = (\alpha - 2\delta^2)^2$, corresponding to $c_1^2 = \delta^2$ or $c_2^2 = \delta^2$, the coefficient q in Eq. (46) vanishes as well. Thus Eq. (46) has two concise roots as before. Specifically, we obtain

$$\lambda' = \frac{\beta}{\delta} + \kappa \pm \frac{1}{|\delta|}\sqrt{\beta^2 - 18\delta^2\beta - 27\delta^4 - 8i\sqrt{\delta^2\beta^3}} \quad (59)$$

for $\beta = \alpha - 2\delta^2 > -\delta^2$ and

$$\lambda' = \frac{\beta}{\delta} + \kappa \pm \frac{1}{|\delta|}\sqrt{\beta^2 + 18\delta^2\beta - 27\delta^4 - 8\sqrt{\delta^2\beta^3}} \quad (60)$$

for $\beta = -\alpha + 2\delta^2 < \delta^2$. Likewise, it is easy to show that in respective allowed regimes of β, the values of λ' given above are always complex, as is the case in Eq. (50) or (51). Also, one can easily find that, as $\beta = 0$ and $\alpha = 2\delta^2$, both Eqs. (59) and (60) can reduce to Eq. (52).

For the other cases, Eq. (46) still can be solved algebraically, although the process is a little cumbersome [39]. We do not present here all four lengthy roots, but just analyze the nature of these roots according to the criterion proposed in Ref. [40]. The criterion says, by example of Eq. (46), that a real-coefficient quartic equation will have four complex roots if and only if the discriminant $\Delta > 0$ and at least one of the conditions $p \geqslant 0$ and $a - p^2/4 > 0$ holds. Clearly, the discriminant Δ of Eq. (46) is found to be

$$\Delta = \frac{4^6(\alpha^2 - \beta^2)[(4\alpha + \delta^2)(\alpha - 2\delta^2)^2 + 27\delta^2\beta^2]^3}{\delta^{10}} > 0, \quad (61)$$

by reason that $\beta^2 < \alpha^2$. Besides, it is easily found that the condition $a - p^2/4 > 0$ holds definitely for $0 < \alpha \leqslant (2 - \sqrt{3})\delta^2$ and $p > 0$ holds for $(2 - \sqrt{3})\delta^2 < \alpha \leqslant (5 + 2\sqrt{6})\delta^2$. As $\alpha > (5 + 2\sqrt{6})\delta^2 \simeq 9.899\delta^2$, we also find that for every α, at least one of the conditions $p > 0$ and $a - p^2/4 > 0$ prevails (see Fig. 3). Hence, according to the criterion above, all four roots of Eq. (46) are complex, of course including the ones responsible for the coupled rogue waves. Recalling the discussion for the equal background case $\beta = 0$, we naturally come to the conclusion that our rogue wave solutions (44) and (45) always exist no matter what parameters have been chosen for the plane-wave seeds (19) and (20). This is quite different from the situation in the integrable Sasa-Satsuma equation where the rogue wave solutions exist only in a limited regime of the starting plane-wave parameters [24].

Despite the complexity of the spectral parameters attributed to unequal backgrounds, one may ask whether such coupled

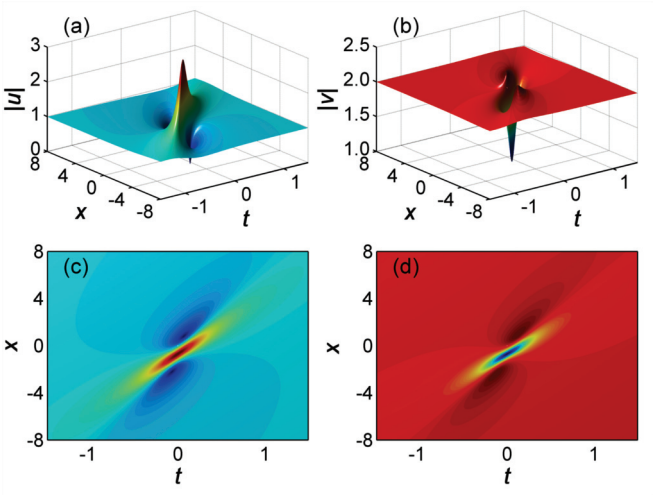

FIG. 4. (Color online) Formation of coupled rogue waves with unequal background amplitude for the starting plane-wave parameters $\epsilon = 0.5$, $k_1 = 1$, $k_2 = 3$, $c_1 = 1$, and $c_2 = 2$. The spectral parameter is given by $\lambda' = 11/2 - (i/2)\sqrt{207 - 48\sqrt{3}}$ according to Eq. (59). (a) and (c) show the u wave and (b) and (d) show the v wave.

rogue waves have more complicated structures than those with equal background amplitude. To answer this question, we simply demonstrate the coupled rogue waves in the following two situations: (i) $c_1 = 1$ and $c_2 = 2$ and, conversely, (ii) $c_1 = 2$ and $c_2 = 1$, with ϵ, k_1, and k_2 the same as in Fig. 2. For the above-specified parameters, one can show that the former situation meets the condition $\beta = \alpha - 2\delta^2$ and hence the spectral parameter is determined by Eq. (59), while the latter goes for $\beta = -\alpha + 2\delta^2$ and thus Eq. (60) applies. The rogue wave solutions are demonstrated in Figs. 4 and 5, respectively, indicating that the above unusual rogue wave structures still exist for such unequal background scenarios. By inspecting the minor details, we note that in Fig. 4 the u and v waves are still centrally humped and sunken, respectively, but both are extended in the x direction as compared to

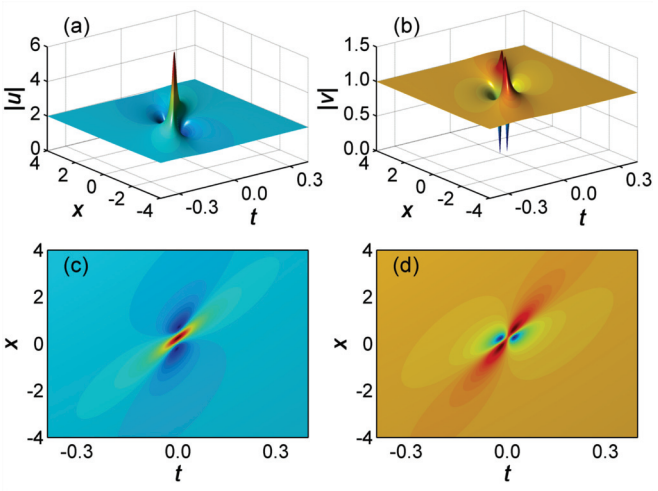

FIG. 5. (Color online) Same as in Fig. 4 except for $c_1 = 2$ and $c_2 = 1$. The corresponding spectral parameter is then given by $\lambda' = 5/2 + (i/2)\sqrt{207 + 48\sqrt{3}}$ according to Eq. (60).

Fig. 2, while in Fig. 5 the u wave is simply amplified in peak amplitude due to the elevation of the background, but the v wave is in a complicated process where its two nearby holes tend to merge.

V. DECOUPLED ROGUE WAVE SOLUTIONS

Finally, we simply discuss the rogue wave solutions as $\delta = 0$. In this case we have

$$k_1 = k_2 = \frac{\kappa}{2}, \tag{62}$$

$$\omega_1 = \omega_2 = \alpha(3\kappa + 2) - \tfrac{1}{8}\kappa^2(\kappa + 2), \tag{63}$$

indicating that the plane-wave seeds (19) and (20) are indeed decoupled in addition to having different amplitude. Similarly, by using the Darboux transformations (17) and (18), we find the rogue wave solutions associated with the spectral parameter $\lambda' = \kappa \pm 4i\sqrt{\alpha}$ as

$$u(t,x) = u_0(t,x)(16\epsilon^2 g - 1), \tag{64}$$

$$v(t,x) = v_0(t,x)(16\epsilon^2 g - 1), \tag{65}$$

where

$$g = \frac{i\alpha(3\kappa + 2)t + 4\epsilon^2}{\alpha^2(3\kappa + 2)^2 t^2 + \alpha\gamma^2 + 16\epsilon^4}, \tag{66}$$

with $\gamma = (\kappa + 3\kappa^2/4 - 6\alpha)t + 4\epsilon x$. This pair of solutions has also been translated along the x axis so that the central maximums are close to the origin. Obviously, Eqs. (64) and (65) are characterized by the same rational function g and thus are decoupled as well. In particular, as $c_1 = 2\epsilon$, $c_2 = 0$, and $k_1 = k_2 = 0$, one can obtain $v = 0$ and the rogue wave solution for the single Hirota equation

$$u = \left[\frac{4(1 + 2it)}{4(x - 6\epsilon t)^2 + 4t^2 + 1} - 1\right] e^{it}, \tag{67}$$

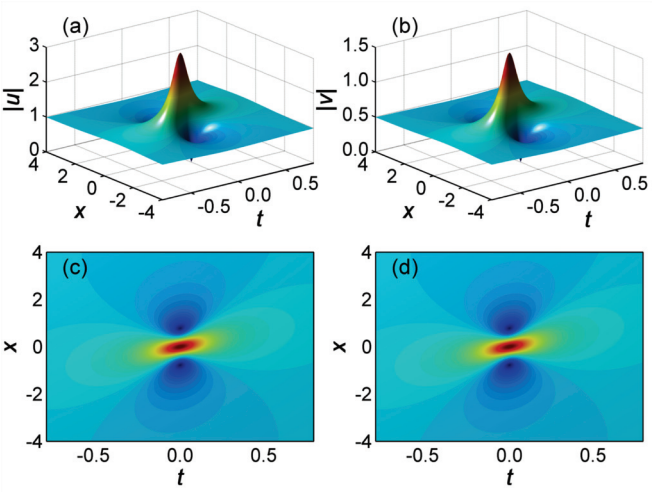

FIG. 6. (Color online) Decoupled rogue waves (64) and (65) associated with $\lambda' = 2 \pm 2i\sqrt{5}$ for the starting plane-wave parameters $\epsilon = 0.5$, $k_1 = k_2 = 1$, $c_1 = 1$, and $c_2 = 0.5$, with ω_1 and ω_2 being given by Eq. (63). (a) and (c) show the u wave and (b) and (d) show the v wave.

which is exactly the same as reported in Ref. [22]. Again, if $\kappa = -2/3$, Eqs. (64) and (65) describe a pair of algebraic solitons on their respective backgrounds [38].

An analysis of the amplitude extremums shows that the decoupled rogue waves (64) and (65) have a peak amplitude three times that of the background at the center (0,0) and two zero-amplitude holes located symmetrically at the points $(0, \sqrt{3/\alpha\epsilon})$ and $(0, -\sqrt{3/\alpha\epsilon})$. Figure 6 demonstrates a pair of decoupled rogue waves formed on different backgrounds [Figs. 6(a) and 6(b)], with their two zero-amplitude points exactly located at $(0, \pm\sqrt{3/5})$ [Figs. 6(c) and 6(d)]. In particular, since the distance between two zero-amplitude points $2\sqrt{3/\alpha\epsilon}$ is not able to be zero by a selection of the seeding parameters, the dark rogue wave structure due to the full merger of two nearby holes, which usually occurs for coupled rogue waves, can never be achieved by decoupled ones.

VI. CONCLUSION

We have presented explicitly exact lowest-order but most general rogue wave solutions of the CH equations by using a Darboux dressing technique. The complex nature of all spectral parameters has been revealed, indicating that our coupled rogue waves, equal or unequal in background height, always exist no matter what parameters have been chosen for the starting plane waves. Several interesting wave characteristics such as the magnitude of the peak amplitude as compared to the significant wave height and the position of two zero-amplitude holes were discussed. We demonstrated that, compared with the decoupled rogue waves that have the same rational form, the coupled rogue waves can appear in a rather striking way, i.e., one wave is humped in the center, while the other exhibits a deep hole there. Calculations showed that such a dark rogue wave structure results from the full merger of two nearby holes as the wave-number difference increases. It is expected that these unusual rogue wave structures due to the two-wave coupling may help explain the extreme wave events in deep ocean [1,2] or in other nonlinear dispersive media where the wave propagation is governed by the CH equations [32–34].

ACKNOWLEDGMENTS

This work was partially supported by the Qing Lan Project, the National Natural Science Foundation of China (Grants No. 10874024 and No. 11174050), the Natural Science Foundation of Jiangsu Province of China (Grant No. BK2011586), and the Scientific Research Foundation for the Returned Overseas Chinese Scholars, SEM.

[1] C. Kharif and E. Pelinovsky, Eur. J. Mech. B Fluids **22**, 603 (2003).
[2] E. Pelinovsky and C. Kharif, *Extreme Ocean Waves* (Springer, Berlin, 2008).
[3] A. Chabchoub, N. P. Hoffmann, and N. Akhmediev, Phys. Rev. Lett. **106**, 204502 (2011).
[4] A. Chabchoub, N. Hoffmann, M. Onorato, and N. Akhmediev, Phys. Rev. X **2**, 011015 (2012); A. Chabchoub, N. Hoffmann, M. Onorato, A. Slunyaev, A. Sergeeva, E. Pelinovsky, and N. Akhmediev, Phys. Rev. E **86**, 056601 (2012).
[5] M. Shats, H. Punzmann, and H. Xia, Phys. Rev. Lett. **104**, 104503 (2010); H. Xia, T. Maimbourg, H. Punzmann, and M. Shats, *ibid.* **109**, 114502 (2012).
[6] D. R. Solli, C. Ropers, P. Koonath, and B. Jalali, Nature (London) **450**, 1054 (2007).
[7] B. Kibler, J. Fatome, C. Finot, G. Millot, F. Dias, G. Genty, N. Akhmediev, and J. M. Dudley, Nat. Phys. **6**, 790 (2010).
[8] C. Lecaplain, Ph. Grelu, J. M. Soto-Crespo, and N. Akhmediev, Phys. Rev. Lett. **108**, 233901 (2012); A. N. Pisarchik, R. Jaimes-Reátegui, R. Sevilla-Escoboza, G. Huerta-Cuellar, and M. Taki, *ibid.* **107**, 274101 (2011).
[9] H. Bailung, S. K. Sharma, and Y. Nakamura, Phys. Rev. Lett. **107**, 255005 (2011).
[10] Yu. V. Bludov, V. V. Konotop, and N. Akhmediev, Phys. Rev. A **80**, 033610 (2009).
[11] Z. Yan, Phys. Lett. A **375**, 4274 (2011).
[12] N. Akhmediev, A. Ankiewicz, and M. Taki, Phys. Lett. A **373**, 675 (2009).
[13] N. Akhmediev, J. M. Soto-Crespo, and A. Ankiewicz, Phys. Lett. A **373**, 2137 (2009).
[14] N. Akhmediev, J. M. Soto-Crespo, and A. Ankiewicz, Phys. Rev. A **80**, 043818 (2009).
[15] Y. C. Ma, Stud. Appl. Math. **60**, 43 (1979).
[16] N. Akhmediev and V. I. Korneev, Theor. Math. Phys. **69**, 1089 (1986).
[17] J. M. Dudley, G. Genty, F. Dias, B. Kibler, and N. Akhmediev, Opt. Express **17**, 21497 (2009).
[18] D. H. Peregrine, J. Aust. Math. Soc. Series B **25**, 16 (1983).
[19] O. C. Wright III, Chaos Solitons Fractals **33**, 374 (2007).
[20] O. C. Wright III, *Hirota Equation, Unstable Plane Waves and Heteroclinic Connections Faculty Summer Grants* (Cedarville University, Cedarville, OH, 2006).
[21] R. Hirota, Phys. Rev. Lett. **27**, 1192 (1971); J. Math. Phys. **14**, 805 (1973).
[22] A. Ankiewicz, J. M. Soto-Crespo, and N. Akhmediev, Phys. Rev. E **81**, 046602 (2010).
[23] Y. Tao and J. He, Rev. Rev. E **85**, 026601 (2012).
[24] U. Bandelow and N. Akhmediev, Phys. Rev. E **86**, 026606 (2012).
[25] Y. Ohta and J. Yang, Rev. Rev. E **86**, 036604 (2012).
[26] F. Baronio, A. Degasperis, M. Conforti, and S. Wabnitz, Phys. Rev. Lett. **109**, 044102 (2012).
[27] Y. V. Bludov, V. V. Konotop, and N. Akhmediev, Eur. Phys. J. Spec. Top. **185**, 169 (2010).
[28] J. He, S. Xu, and K. Porseizan, Rev. Rev. E **86**, 066603 (2012).
[29] J. M. Soto-Crespo, Ph. Grelu, and N. Akhmediev, Phys. Rev. E **84**, 016604 (2011); A. Zaviyalov, O. Egorov, R. Iliew, and F. Lederer, Phys. Rev. A **85**, 013828 (2012).

[30] D. R. Solli, C. Ropers, and B. Jalali, Phys. Rev. Lett. **101**, 233902 (2008).
[31] T. B. Benjamin and J. E. Feir, J. Fluid Mech. **27**, 417 (1967); V. P. Ruban, Phys. Rev. Lett. **99**, 044502 (2007).
[32] R. S. Tasgal and M. J. Potasek, J. Math. Phys. **33**, 1208 (1992).
[33] R. Radhakrishnan, M. Lakshmanan, and M. Daniel, J. Phys. A: Math. Gen. **28**, 7299 (1995).
[34] K. Porsezian and K. Nakkeeran, Pure Appl. Opt. **6**, L7 (1997); S. G. Bindu, A. Mahalingam, and K. Porsezian, Phys. Lett. A **286**, 321 (2001).
[35] G. P. Agrawal, *Nonlinear Fiber Optics*, 4th ed. (Academic, San Diego, 2007).
[36] G.-Q. Xu, Phys. Rev. E **74**, 027602 (2006).
[37] D. Mihalache, N. Truta, and L.-C. Crasovan, Phys. Rev. E **56**, 1064 (1997).
[38] G. I. Burde, Phys. Rev. E **84**, 026615 (2011).
[39] *Handbook of Mathematical Functions with Formulas, Graphs, and Mathematical Tables*, edited by M. Abramowitz and I. A. Stegun (Dover, New York, 1972), Chap. 3.8.3.
[40] E. L. Rees, Am. Math. Mon. **29**, 51 (1922).